

An oscillatory hierarchy controlling cortical excitability and stimulus processing

Peter Lakatos^{1,2}, Ankoor S. Shah^{1,4}, Kevin H. Knuth³, Istvan Ulbert², George Karmos², and Charles E. Schroeder^{1,4}

¹ *Cognitive Neuroscience and Schizophrenia Program, Nathan Kline Institute, Orangeburg, New York 10962,*

² *Institute for Psychology, Hungarian Academy of Sciences, Budapest, H-1394,*

³ *Computational Sciences Division, Code TC, NASA Ames Research Center, Moffett Field, California 94035-1000,*

⁴ *Department of Neuroscience, Albert Einstein College of Medicine, Bronx, New York 10461*

Electroencephalographic (EEG) oscillations are hypothesized to reflect cyclical variation in the excitability of neuronal ensembles [1], with particular frequency bands reflecting differing types [2-4] and spatial scales [5-7] of brain operations. Interdependence between the gamma and theta bands [5, 8] suggests an underlying structure to the EEG spectrum, and there is also evidence that ongoing activity influences sensory responses [9, 10]. However, there is no unifying theory of EEG organization and the role of the ongoing oscillatory activity in sensory processing remains controversial. This study analyzed laminar profiles of synaptic activity and action potentials, both spontaneous and stimulus-driven, in primary auditory cortex [11]. We find that - 1) The EEG is hierarchically organized; delta (1-4 Hz) phase modulates theta (4-10 Hz) amplitude, and theta phase modulates gamma (30-50 Hz) amplitude. 2) This Oscillatory Hierarchy controls baseline excitability and action potential generation, as well as stimulus-related responses in a neuronal ensemble. We propose that the hierarchical organization of ambient oscillatory activity allows auditory cortex to structure its temporal activity pattern so as to optimize the processing of rhythmic inputs.

Laminar profiles of field potentials (EEG) and concomitant multiunit action potentials (MUA) were recorded during 25 experiments in 4 awake rhesus monkeys, using a linear array multi-contact electrode (100 μm intercontact spacing) positioned to sample from all the layers simultaneously [11](Fig.1A). Rather than analyzing the field potential itself, our analyses were applied to its second spatial derivative, the current source density (CSD) profile (Fig. 1B; methods), because this approach eliminates effects of volume conduction and allows more direct interpretation of field potential oscillations in terms of the underlying synaptic activity in the local neuronal ensemble [12, 13].

Spontaneous rhythmic activity was observed in all cortical layers, but four locations had higher amplitude oscillations than the surrounding ones (Fig. 1C. and 1D.). Two of these locations were in the supragranular layers (‘S₁’ and ‘S₂’), one in the granular layer (‘G₁’) and one in the infragranular layers (‘I₁’). Across penetrations, mean distance was 324 μm between the S₁- S₂ (STD=88), 488 μm between the S₂- G₁ (STD=112) and 364 μm (STD=86) between the G₁- I₁ electrodes. Subsequent analyses focused on these sites. The spontaneous CSD in each site contained three spectral peaks, in the delta, theta and gamma frequency ranges; this is illustrated using the amplitude spectrum of the S₂ site (Fig 2A, upper). As shown in figure 1D, amplitudes of theta and delta oscillations in the supragranular layers were significantly greater than in granular and infragranular layers ($p < 0.05$). There was no significant difference in gamma amplitude in the supragranular and granular layers ($p > 0.05$), but it was significantly smaller in the infragranular layers ($p < 0.05$). Across layers, the mean frequency of oscillation within each band did not differ significantly ($p > 0.05$).

In the spontaneous activity, theta and gamma frequency oscillation currents showed large periodic amplitude fluctuations, and these had systematic patterns: gamma oscillation current density fluctuated at theta frequency, while the theta oscillation

current density fluctuated at delta frequency. Further, the highest amplitude theta oscillations occurred at a specific (bursting) phase of the delta oscillation and the same relationship held between the gamma oscillation amplitude and the theta oscillation phase. This is illustrated using activity from the S₂ site (Fig. 2B, upper). These effects occurred in all layers, but were greatest in supragranular sites. We noted a periodic 0.05-0.2 Hz fluctuation in the amplitude of the delta waves, but technical constraints (data were digitized after passing the analog signal through a high-pass filter with a corner frequency of 0.1 Hz) precluded quantitative analysis here.

We also examined the relationship between the phase of delta, theta and gamma frequency oscillation currents and MUA (Fig. 2B, lower). There was a clear phase related modulation of the MUA in all the layers, with the modulation being greatest in the granular layer. In the case of delta and theta oscillations, the phase with maximal MUA (firing phase) appeared to lag slightly behind the bursting phase, but there was no significant difference between the two angular means ($p > 0.05$).

Like the spontaneous spectrogram, that of the event-related CSD at the peak of the initial transient cortical response had three clear amplitude maxima; the event-related spectrogram for the S₂ site is used for illustration (Fig. 3A). There were no significant differences between spontaneous and stimulus driven conditions in the frequencies of theta and gamma oscillations, however, the mean frequency of delta oscillations was significantly lower in the latter condition ($p < 0.05$). Strikingly, the peak frequency of stimulus-related delta oscillation was a near perfect match to the stimulus rate; in 22 out of 25 experiments the peak frequency in the delta band during stimulation was 1.33 Hz (the stimulation rate). Stimulus-related theta and gamma oscillations were significantly larger ($p < 0.05$) than the spontaneous oscillatory amplitudes, but the amplitude of the delta oscillations was significantly smaller ($p < 0.05$). While there was a

clear pre- to post-stimulus amplitude increase in the theta and gamma range, the amplitude of the delta oscillation showed no stimulus-related change (Fig. 3B.).

These results indicate that although there was no stimulus evoked delta oscillation, the frequency of the ongoing delta waves rapidly adapted or “entrained” to the stimulation frequency (Fig. 3C.). While the first stimulus in a train was associated with random delta phase (Rayleigh’s uniformity test, $p < 0.05$, $n = 25$), repetitive rhythmical stimulation resulted in a non-uniform pre-stimulus (0 ms) delta phase distribution in the rest of the trials (Rayleigh’s uniformity test, $p < 0.05$, $n = 149$) in all 25 experiments.

Do the oscillatory fluctuations in excitability described above have an impact on stimulus processing? To address this question, we analyzed the effect of pre-stimulus delta phase on the stimulus-related CSD and MUA. We found that the amplitude of the evoked response is dependent on the phase of ongoing delta oscillation. This is illustrated in 2 ways for a single experiment (Fig. 4A. and B.). Figure 4A shows the distribution of single trial response amplitudes (CSD, left and MUA, right) as a function of delta phase. Figure 4B shows the laminar profile of response (CSD with superimposed MUA) to a pure tone, averaged across trials with delta phase corresponding to the largest post-stimulus activation (left) and smallest post-stimulus activation (right). Effects were quantified across experiments using a Modulation Index (Fig. 4C).

Delta phase was systematically related to stimulus-evoked response amplitude in all the cortical layers, with the modulation being largest in the supragranular layers. The “ideal” pre-stimulus phase, which resulted in the biggest event related activation (ϕ mean=1.98 rad, ϕ dev=0.88) was counter-phase to the “worst” phase, which resulted in

the smallest event related CSD and MUA (ϕ mean=-1.54 rad, ϕ dev=1.09); the ideal phase also corresponded to the bursting phase of the spontaneous delta oscillation.

Laminar differences in delta phase dependence are noteworthy. The extreme extent of delta phase dependence in the superficial layers indicates that processing in these layers is determined largely by context, that is, the instantaneous “state” cortex in which inputs arrive. By contrast, the granular layer response appears to be determined mostly by the input.

An early hypothesis [1] suggested that spontaneous EEG reflects rhythmic variation of cortical excitability. Although the relationship of the EEG to neuronal activity was relatively neglected over the intervening years, recent studies have re-kindled interest in this topic. Intracellular recordings in carnivores provided a striking demonstration of neuronal membrane potentials undergoing slow rhythmic shifts between depolarized and hyperpolarized states during slow wave sleep [14, 15]. Other recent findings have pointed to an underlying structure to the EEG spectrum. In humans, cats and rats, for example, higher frequency oscillations display amplitude fluctuations with periodicity matching that of lower frequency oscillations [16-20]. Moreover, dependence of gamma oscillation amplitude on theta oscillatory phase is well characterized in rodent hippocampus [8, 21] and entorhinal cortex [22, 23]. Finally, there is gathering evidence that sensory processing is heavily influenced by ongoing cortical activity, as measured by optical imaging [24], and ERPs [10].

The present study provides a way to organize these important findings. First, we show that there is a hierarchical structure to the EEG, with amplitude at each oscillatory frequency being modulated by the phase of a lower frequency oscillation. This structure appears to extend from slow waves up through the gamma frequencies, although technical constraints precluded quantitative assessment of the inter-relationship of delta

and very slow oscillations. There is also indication of additional facets of EEG structure, beyond those described here; these issues will require further experimentation. Earlier findings from intracellular recordings *in-vitro* suggest that Layer 5 pyramidal cells play a key role in organizing and promoting slow oscillations in cortical neurons [14]. The fact that in our recordings, delta and theta oscillations are by far largest in the supragranular layers suggests that the pyramidal neuron ensembles there are also important in controlled cortical processing. The relationship between these findings remains to be established. A second key aspect of our findings is that like the slow oscillation, the higher frequency oscillations reflect concerted excitability variations in cortical ensembles. This is reflected in local neuronal firing (MUA) which is clearly related to the phase of delta, theta and gamma oscillations.

Finally, we confirm that ambient oscillatory activity has significant effects on stimulus processing, in that, for each band of oscillation, there are both ideal and worst phases, during which stimulus responsiveness is enhanced or suppressed. While stimulus processing clearly is structured by the ambient “context,”[24] the onset of a sound can instantly re-set the phase of the ambient delta oscillation, which effectively phase-locks the entire hierarchical structure of oscillatory activity to the stimulus. This effect should be enormously useful in processing sounds that occur with a period of 1-4 Hz, and have relatively phase-locked, rhythmic components at 4-10 Hz (theta) and 30-50 Hz (gamma). It so happens that for primates, including humans, the temporal structure of numerous biologically-relevant stimuli [25], especially vocalizations [26, 27], fit this pattern remarkably well.

Methods

Surgery. 4 male macaques (*Macaca mulatta*), weighing 5-7 kg were subject were prepared for chronic awake electrophysiological recording. Surgery was performed under anesthesia (1-2% isoflurane), using standard aseptic surgical methods [11]. All procedures were approved in advance by the Animal Care and Use Committee of the Nathan Kline Institute. Prior to surgery, each animal was adapted to a custom fitted primate chair and to the recording chamber.

Electrophysiological recording. Recordings were made in an electrically shielded, sound-attenuated chamber lined with SONEX ProSPEC Composite™ sound absorbing foam. In this study, the subjects were conditioned to sit quietly, but were not required to attend or respond to the stimuli. During recording, subjects were monitored continuously using electroencephalographic recording (EEG) and infrared video, and were kept in an alert state by interacting with them. Only recordings with no movement were analyzed. Auditory stimuli consisted of 70dB SPL 100ms (4ms rise/fall time) Gaussian noise bursts and pure tones (frequencies: 0.5kHz, 1kHz, 2 kHz, 4 kHz, 8 kHz, 16 kHz and 20 kHz) produced using Tucker Davis Technology's System III coupled with ES-1 speakers. For optimal implementation of CSD analysis, during each experiment, a linear-array multi-contact electrode (24 contacts, electrode spacing 100 μm , Fig. 1A.) was lowered into auditory cortex perpendicular to the lamination pattern, as determined by pre-implant MRI [28]. The laminar CSD profile evoked by binaural Gaussian noise bursts was used to position the electrode array to straddle the cortex from the pial surface to the white matter [11]. Once the position was refined, it was left stable for the duration of recording. At the beginning of each experimental session, after determining the best frequency using a tonotopy paradigm (random frequency pure tones and gaussian noise), we recorded 2 minutes of spontaneous activity followed by an approximately 2 minutes long stimulus train ($n=150$) consisting of the best frequency pure tone with an inter-stimulus interval of 767 ms. Laminar activity profiles consisting of concomitant field potentials and multiunit activity (MUA) were obtained during the

experiments. Signals were impedance matched with a pre-amplifier (10x gain, bandpass dc-10 kHz) situated on the electrode, and after further amplification (500x) the signal was split into field potential (0.1-500Hz) and MUA (300-5000Hz) range by analog filtering. Field potentials were sampled at 2kHz/16bit precision, MUA was sampled at 20kHz/12bit precision. Additional zero phase shift digital filtering (300-5000Hz) and rectification was applied on the MUA data to extract the continuous estimate of cell firing.

Data analysis. Data were analyzed offline using Matlab (Mathworks, Natick, MA). One-dimensional CSD profiles were calculated from the spatially smoothed (Hamming window) local field potential profiles using a three-point formula for estimation of the second spatial derivative of voltage [29]. CSD analysis provides an index of the location, direction, and density of transmembrane current flow; this is the first-order neuronal response to synaptic input [28]. After selectively averaging the CSD and MUA responses to a series of seven randomly presented pure tones ranging from 0.5 to 20 kHz (suprathreshold tonotopy paradigm, [11, 30]), we functionally assigned each recording site to A1 versus belt auditory cortex, and determined the region's characteristic response frequency (best frequency). In the present study only recordings obtained from area A1 were used. Our data set consisted of two parts: 1) 2 minute long spontaneous recordings and 2) event related responses evoked by a stimulus train (n=150, ISI=767) of best frequency pure tones (also recorded continuously and epoched off-line from -2000 to 2000 ms). For the analysis of spontaneous and event related oscillations, instantaneous power and phase were extracted by wavelet decomposition (Morlet wavelet) on 84 scales from 1 to 101.2 Hz. After applying the wavelet transformation we calculated the square root of the power values to estimate the amplitude of the local oscillation currents. To compute oscillatory amplitude or MUA as a function of oscillatory phase, we sorted the phase values obtained from the wavelet transformation for the entire 2 minute recording from $-\pi$ to π radians. Then we

applied the permutation vector obtained from sorting the phases to the oscillatory amplitude values and the MUA for the same segment. The data was then down-sampled to 360 data points. Pooled amplitude and frequency values were evaluated statistically by ANOVA. When significant changes were detected with ANOVA, multiple comparisons (Statistical Toolbox of Matlab) were used to determine which pairs of means were significantly different. Phase values were analyzed by circular statistics methods. Pooled phases were compared using the Watson U^2 test for circular data. Significant deviation from uniform (random) phase distribution was tested with Rayleigh's uniformity test.

1. Bishop, G., *Cyclical changes in excitability of the optic pathway of the rabbit*. Am J Physiol, 1933. **103**: p. 213-224.
2. Singer, W. and C.M. Gray, *Visual feature integration and the temporal correlation hypothesis*. Annu Rev Neurosci, 1995. **18**: p. 555-86.
3. Kahana, M., D. Seelig, and J. Madsen, *Theta returns*. Current Opinions in Neurobiology, 2001. **11**: p. 739-744.
4. Buzsaki, G. and A. Draguhn, *Neuronal oscillations in cortical networks*. Science, 2004. **304**: p. 1926-1929.
5. Steriade, M., *Impact of network activities on neuronal properties in corticothalamic systems*. J. Neurophysiol., 2001. **86**: p. 1-39.
6. Leopold, D., Y. Murayama, and N. Logothetis, *Very slow activity fluctuations in monkey visual cortex: Implications for functional brain imaging*. Cerebral Cortex, 2003. **12**: p. 422-433.
7. Csicsvari, J., et al., *Mechanisms of gamma oscillations in the hippocampus of the behaving rat*. Neuron, 2003. **37**: p. 311-322.

8. Bragin, A., et al., *Gamma (40-100Hz) Oscillation in the hippocampus of the behaving rat*. J. Neurosci., 1995. **15**: p. 47-60.
9. Arieli, A., et al., *Coherent spatiotemporal patterns of ongoing activity revealed by real-time optical imaging coupled with single-unit recording in cat visual cortex*. J. Neurophysiol., 1995. **73**: p. 2072-2093.
10. Kruglikov, S.Y. and S.J. Schiff, *Interplay of electroencephalogram phase and auditory evoked neural activity*. J. Neurosci., 2003. **23**(10122-10127).
11. Schroeder, C.E., et al., *Somatosensory input to auditory association cortex in the macaque monkey*. J Neurophysiol, 2001. **85**(3): p. 1322-7.
12. Nicholson, C., *Theoretical analysis of field potentials in anisotropic ensembles of neuronal elements*. IEEE Trans. Biomed. Engin, 1973: p. BME-20 278-288.
13. Schroeder, C.E., et al., *Localization of ERP generators and identification of underlying neural processes*. Electroencephalogr Clin Neurophysiol Suppl, 1995. **44**: p. 55-75.
14. Sanches-Vives, M. and D.A. McCormick, *Cellular and network mechanisms of rhythmic recurrent activity in the neocortex*. Nat Neurosci, 2002. **3**: p. 1027-1034.
15. Steriade, M., D.A. McCormick, and T.J. Sejnowski, *Thalamocortical oscillations in the sleeping and aroused brains*. Science, 1993. **262**: p. 679-685.
16. Amzica, F. and M. Steriade, *Cellular substrates and laminar profile of sleep K-complex*. Neuroscience, 1998. **82**: p. 671-686.
17. Freeman, W.J. and L.J. Rogers, *Fine temporal resolution of analytic phase reveals episodic synchronization by state transitions in gamma EEGs*. J. Neurophysiol., 2002. **87**: p. 937-945.
18. Vanhatalo, S., et al., *Infraslow oscillations modulate excitability and interictal epileptic activity in the human cortex during sleep*. PNAS, 2004. **101**(14): p. 5053-5057.

19. Steriade, M., et al., *Synchronization of fast (30-40 Hz) spontaneous oscillations in intrathalamic and thalamocortical networks*. J. Neurosci., 1996. **16**: p. 2788-2808.
20. Lakatos, P., et al., *Attention and arousal related modulation of spontaneous gamma activity in the auditory cortex of the cat*. Cogn. Brain Res., 2004. **19**: p. 1-9.
21. Buzsaki, G., et al., *Hippocampal network patterns of activity in the mouse*. Neuroscience, 2003. **116**: p. 201-211.
22. Cunningham, M.O., et al., *Gamma oscillations induced by kainate receptor activation in the entorhinal cortex in vitro*. J. Neurosci., 2003. **23**: p. 9761-9769.
23. Chrobak, J.J., A. Lorincz, and G. Buzsaki, *Physiological patterns in the hippocampo-entorhinal system*. Hippocampus., 2000. **10**: p. 457-465.
24. Arieli, A., et al., *Dynamics of ongoing activity: explanation of the large variability in evoked cortical responses*. Science, 1996. **273**: p. 1868-1871.
25. Singh, N. and F. Theunissen, *Modulation spectra of natural sounds and ethological theories of auditory processing*. J. Acoust Soc. Am., 2003. **114**: p. 3394-3411.
26. Shannon, R., et al., *Speech recognition with primarily temporal cues*. Science, 1995. **270**: p. 303-304.
27. Wang, X., et al., *Representation of a species-specific vocalization in the primary auditory cortex of the common marmoset: temporal and spectral characteristics*. J Neurophysiol, 1995. **74**(6): p. 2685-706.
28. Schroeder, C.E., A.D. Mehta, and S.J. Givre, *A spatiotemporal profile of visual system activation revealed by current source density analysis in the awake macaque*. Cereb Cortex, 1998. **8**(7): p. 575-92.

29. Nicholson, C. and J.A. Freeman, *Theory of current source density analysis and determination of conductivity tensor for anuran cerebellum*. Journal of Neurophysiology, 1975. **38**: p. 356-368.
30. Steinschneider, M., et al., *Physiologic correlates of the voice onset time (VOT) boundary in primary auditory cortex (A1) of the awake monkey: temporal response patterns*. Brain and Language, 1995. **48**: p. 326-340.

Acknowledgments: We thank Dr. Gyorgy Buzsaki and his laboratory for helpful discussions of methods and theory, and Dr. Zsuzsa Pincze for her helpful comments on an earlier version of the manuscript. We also thank Tammy McGinnis, Monica O'Connell and Aimee Mills for their invaluable assistance in collecting the data.

Correspondence and requests for materials should be addressed to C.E. Schroeder, Ph.D. (e-mail: schrod@nki.rfmh.org)

Figure 1 - Laminar profile of the amplitude of spontaneous oscillation currents in area AI. A Linear array multielectrode (100 μ m intercontact spacing) positioned to sample from all cortical layers. **B** Current source density (CSD) map of a characteristic spontaneous activity segment (1.5 seconds). Current sinks (red) represent net inward transmembrane current flow in the local neuronal ensemble; sources (blue) represent outward currents. **C**

Laminar amplitude profiles of the spontaneous oscillation currents show two maxima in the supragranular layers ('S₁' and 'S₂'), one in the granular ('G₁') and one in the infragranular layers ('I₁'). **D)** Pooled data (n=25) for the amplitude of spontaneous oscillations (bars represent standard error).

Figure 2 - Phase, amplitude and MUA relationships of the spontaneous

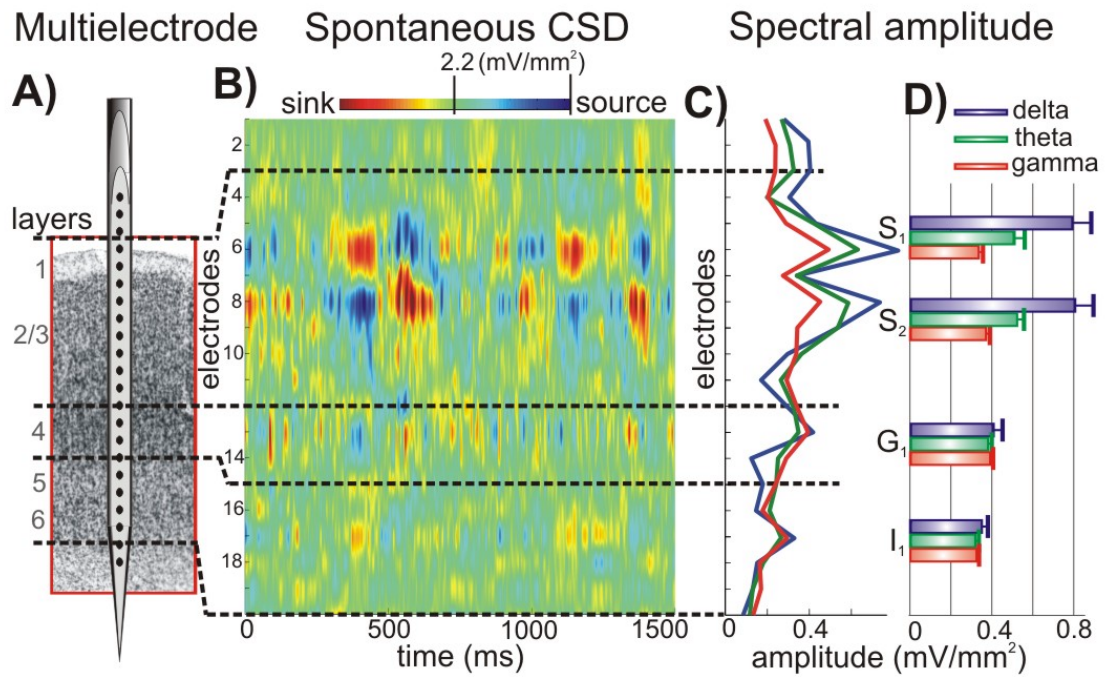
oscillation currents. A) Wavelet amplitude spectrum of spontaneous oscillations recorded from the lower supragranular electrode (S₂). Box and whisker plots (box has lines at lower quartile, median, and upper quartile values, while whiskers show the extent of the data) show pooled data (n=25) for the amplitude and frequency of the maxima of spontaneous oscillation currents. Table shows pooled data for all four laminar sites (S₁, S₂, G₁ and I₁). **B)** Upper two traces show delta modulation of theta amplitude (blue trace) and theta modulation of gamma amplitude (green trace). Lower three traces show modulation of MUA by the phase of the different frequency oscillations (delta - blue, theta - green, gamma - red). Table shows pooled data of the bursting and firing phases for all sites (S₁, S₂, G₁ and I₁).

Figure 3 - Event-related oscillations. A) Wavelet amplitude spectrum of stimulus-related CSD at the lower supragranular site (S₂). Box and whisker plots show pooled data (n=25) for the amplitude maxima and frequency of event-related oscillation currents. Outliers are marked by a red cross. **B)** Pooled single trial wavelet amplitudes of event-related delta, theta and gamma oscillation currents. (apparent pre-stimulus amplitude increase is a side-effect of the temporal smearing caused by the wavelet transformation.) **C)** Stacked bars on the left show the phase of delta oscillation for the first trial in the trial block for all

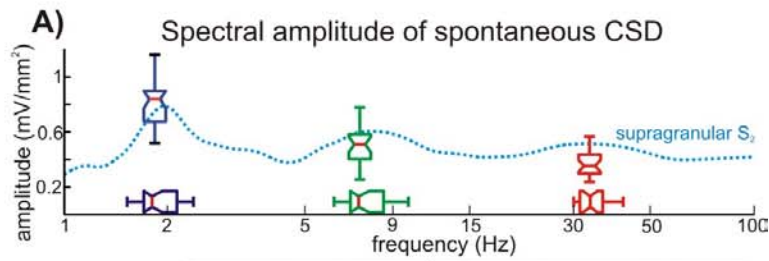
experiments (n=25) at the time of stimulus presentation (0 ms). Stacked bars on the right show pooled data of delta phase for all succeeding trials. The number of trials is normalized to the total number of trials (excluding the first, n=149) in each experimental session. The colors in both graphs represent the experimental sessions.

Figure 4 - Delta phase dependence of the event-related response. **A)** Mean rectified event-related CSD and MUA amplitudes for the 10-100 ms time interval for trials with different delta phase. **B)** Event-related CSD profiles evoked by the best frequency tone; left - average of trials with delta phase corresponding to the largest post-stimulus activation; right - average of trials with delta phase corresponding to the smallest post-stimulus activation. Overlaid traces show MUA. **C)** Pooled data (n=25) showing the modulation index (ratio of the ideal phase response over the worst phase response) for all cortical layers.

Schroeder_fig1

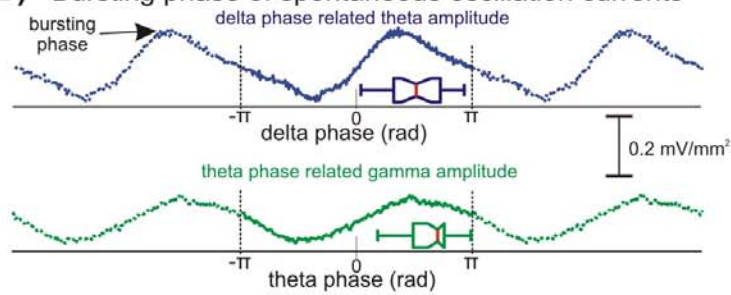


Schroeder_fig2

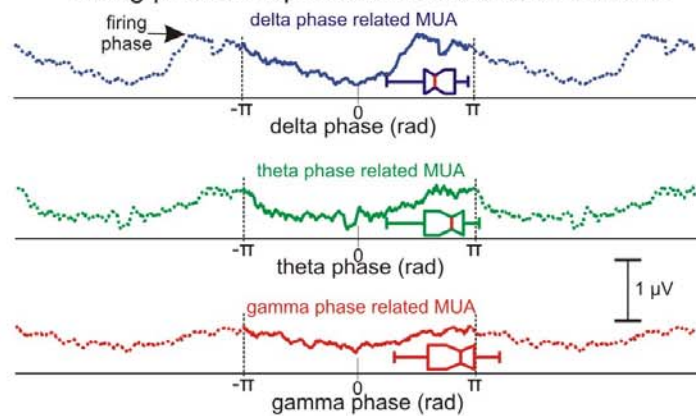


electrode	amplitude (mV/mm ²)				frequency (Hz)				
	S ₁	S ₂	G ₁	I ₁	S ₁	S ₂	G ₁	I ₁	
delta	mean	0.81	0.83	0.41	0.37	1.84	1.86	1.89	1.83
	sd	0.19	0.12	0.06	0.08	0.23	0.25	0.29	0.31
theta	mean	0.52	0.53	0.38	0.33	7.50	7.51	7.71	7.53
	sd	0.16	0.13	0.08	0.08	0.93	1.03	1.33	1.13
gamma	mean	0.34	0.37	0.39	0.34	34.81	34.51	35.61	35.31
	sd	0.11	0.07	0.08	0.06	3.53	3.30	3.31	3.93

B) Bursting phase of spontaneous oscillation currents

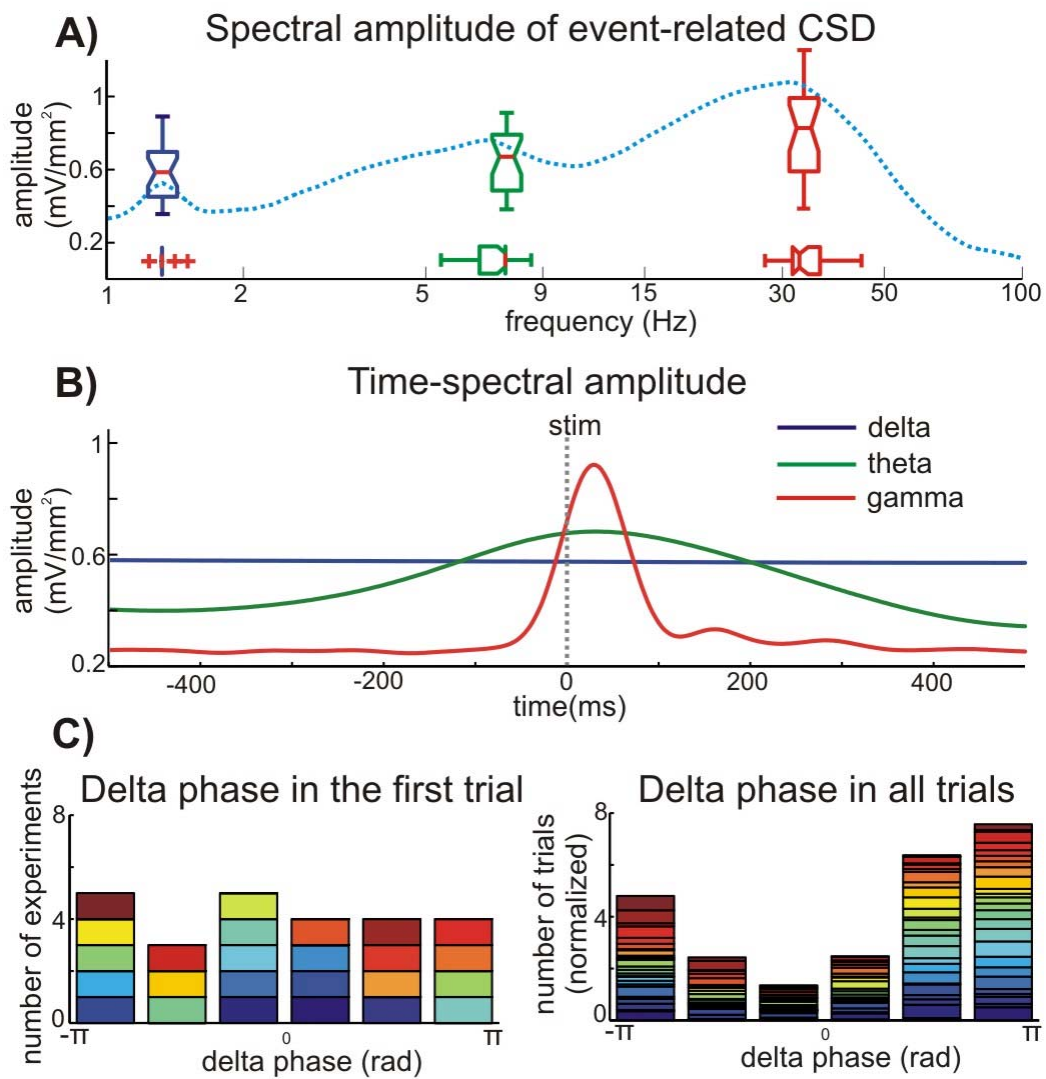


Firing phase of spontaneous oscillation currents



electrode	bursting phase (rad)				firing phase (rad)				
	S ₁	S ₂	G ₁	I ₁	S ₁	S ₂	G ₁	I ₁	
delta	φ mean	-1.36	1.62	2.84	-0.37	-1.68	2.22	2.89	-0.48
	φ dev	0.86	0.84	1.01	1.03	0.91	0.54	0.71	0.83
theta	φ mean	-0.51	2.00	2.34	-1.27	-1.00	2.51	2.76	-1.20
	φ dev	0.82	0.81	1.01	1.12	1.64	0.64	1.10	1.42
gamma	φ mean					-0.27	2.81	3.02	-0.19
	φ dev					1.11	0.76	0.69	1.44

Schroeder_fig3



Schroeder_fig4

